Journal of Solid State Chemistry **153,** 391–397 (2000)
doi:10.1006/jssc.2000.8788, available online at http://www.idealibrary.com on IDEAL®

$CaAl_{12}Si_4O_{27}$, a New High-Pressure Phase Containing Al_6O_{19} Clusters

I. E. Grey,*,[1] I. C. Madsen,* W. O. Hibberson,† and H. St. C. O'Neill†

*CSIRO Minerals, Box 312, Clayton South 3169, Australia; and †Research School of Earth Sciences, Australian National University, Canberra 0200, Australia

Received February 4, 2000; in revised form May 24, 2000; accepted May 24, 2000; published online July 26, 2000

$CaAl_{12}Si_4O_{27}$, a new high-pressure phase in the $CaO–Al_2O_3–SiO_2$ system, was prepared at 1550°C and 14 GPa. It has trigonal symmetry, *P*-3, with $a = 7.223(1)$ and $c = 8.614(3)$ Å. Its structure was solved using crystal chemistry principles and refined using the Rietveld method applied to powder X-ray diffraction data, $R_{wp} = 6.1\%$, $R_B = 2.7\%$. The structure is a new type based on a close-packed anion lattice with a mixed layer stacking sequence $ABACA \equiv (hc)_2$ and with Ca atoms ordered in one-seventh of the anion sites in alternate *c*-stacked layers. The Si atoms are ordered in both octahedral and tetrahedral sites while the Al atoms are ordered in two independent octahedral sites. Octahedral edge-shared clusters, Al_6O_{19}, occur in the structure, interconnected within the close-packed layers by corner-linking to SiO_4 tetrahedra. The clusters are also connected by corner-sharing to nine-member rings of edge-shared Al- and Si-centered octahedra in adjacent layers. The new phase has structural features in common with the barium titanium ferrite of similar composition, $BaFe_{11}Ti_3O_{23}$, as well as with the mineral simpsonite, $Al_4Ta_3O_{13}(OH)$, and alkali metal niobates which contain Nb_6O_{19} clusters. © 2000 Academic Press

INTRODUCTION

We recently reported the structural characterisation of the new high-pressure (HP) phase $CaAl_4Si_2O_{11}$ in the $CaO–Al_2O_3–SiO_2$ system, obtained at 14 GPa and 1600°C (1). Our results agreed with those of an independent study by Gautron *et al.* (2) that confirmed that the new phase was isostructural with the R-type hexagonal ferrite, $BaFe_4Ti_2O_{11}$ (3). The HP preparations of $CaAl_4Si_2O_{11}$ always showed the presence of a few percent of grossular garnet together with a small amount of an unidentified phase.

By varying the atomic proportions in different HP syntheses we were able to increase the amount of the unidentified phase to the point where we were able to obtain an estimate of its composition from electron microprobe analyses as $CaAl_{10}Si_4O_{24}$. The powder X-ray diffraction (PXRD) pattern for the new phase did not correspond to any known structure type, but the strongest peaks were similar to those in the PXRD pattern of another barium titanium ferrite, $BaFe_{11}Ti_3O_{23}$ (4). This information, coupled with crystal chemical reasoning, was used to determine the structure of the new phase. The structure determination allowed the composition to be established as $CaAl_{12}Si_4O_{27}$, The structure was refined using the Rietveld method applied to the PXRD data. The structure determination revealed that while $CaAl_{12}Si_4O_{27}$ has the same type of anion close-packing in common with the ferrite phase, the cation lattice is quite different; in particular the new structure contains Al_6O_{19} octahedral clusters. In this paper we report the determination and refinement of the structure for $CaAl_{12}Si_4O_{27}$ and discuss its relationship to other close-packed structures.

EXPERIMENTAL

High-Pressure Syntheses

Starting materials for the preparations were analytical grade $CaCO_3$, $Al(OH)_3$, and silicic acid, $SiO_2.xH_2O$. Appropriately weighed mixtures of these compounds were homogenized by grinding under acetone in an agate mortar and then transferred to a platinum crucible and heated slowly to drive off CO_2 and H_2O. The mixtures were then melted on an iridium strip heater and quenched to form glasses of different $CaO:Al_2O_3:SiO_2$ molar compositions. The glasses generally contained small crystals that exsolved during quenching. The bulk compositions were checked by electron microprobe analysis, using a defocused beam to include both glass and quench crystals.

Crystalline phases were synthesized from the glasses at a pressure of 14 GPa and at temperatures in the range 1550 to 1650°C in an MA8-type multianvil apparatus, a full description of which is given by Ohtani *et al.* (5). Temperatures were measured using W97Re3–W75Re25 thermocouples. Aliquots of typically 2 to 3 mg of finely ground glass were loaded into platinum capsules and sealed for the high-pressure experiments. Runs were quenched by turning

[1]To whom correspondence should be addressed. Fax: 613 9562 8919. E-mail: ian.grey@minerals.csiro.au.

0022-4596/00 $35.00
Copyright © 2000 by Academic Press
All rights of reproduction in any form reserved.

off the power and then slowly decompressed over a period of 12 h.

Powder X-Ray Diffraction

The high-pressure products were extracted under a binocular microscope, finely ground using a boron nitride micromortar, and loaded into 0.3 mm diameter Lindeman glass capillaries. X-ray intensity data were collected on an Inel diffractometer fitted with a CPS120 position-sensitive detector, and with a multilayer mirror to provide both high intensity and a parallel beam. Vertical and horizontal slits were set at 0.15 mm and 4 mm, respectively. A copper tube was operated at 35 kV and 35 mA. The detector was positioned to collect data in the 2θ range 16 to 136°. Data collection times were typically 24 h.

Structure refinements were carried out using the Rietveld program CSRIET/SR5, a local CSIRO Minerals modification of the code by Hill and Howard (6) and Wiles and Young (7) which allows for quantitative phase analysis of multiphase mixtures. Refined profile parameters included scale factors for each phase present, pseudo-Voigt peak shape parameters, two parameters of a full width at half-maximum function (8), a 2θ zero-error, and the unit cell parameters. The background was interpolated from 27 direct measurements made along the pattern. X-ray scattering factors for ionized atoms were taken from the *International Tables for X-Ray Crystallography* (9).

Structure Determination

Electron microprobe analyses of crystals of the new phase, associated with $CaAl_4Si_2O_{11}$ and garnet, gave an approximate composition $CaAl_{10}Si_4O_{24}$. Indexing of the PXRD pattern of the new phase and refinement of the unit cell parameters were accomplished using the program ITO (10), giving the hexagonal cell parameters $a = 7.223(1)$ and $c = 8.614(4)$ Å. The structure was determined by using crystal chemistry reasoning. We had previously shown, in agreement with the prediction of Gautron *et al.* (2), that the HP phase $CaAl_4Si_2O_{11}$ was isostructural with the barium titanium ferrite $BaFe_4Ti_2O_{11}$ (1). We explored the possibility of extending the analogy to the new phase. In the BaO–Fe_2O_3–TiO_2 system, there is a ternary phase at the molar composition 1:5.5:3 (4) which is quite close to that analyzed for the new phase. Using the published structure parameters we calculated the PXRD pattern for the ferrite, $BaFe_{11}Ti_3O_{23}$. Although it differed in detail from the experimental pattern for the HP phase, the two PXRD patterns had in common the positions of the strongest reflections which correspond to diffraction from the O + Ba close-packed array for the ferrite.

In $BaFe_{11}Ti_3O_{23}$ the anion close-packing has an eight-layer stacking sequence involving an alternation of cubic and hexagonal stacking, $(ch)_4$, with the large Ba cations ordered at anion sites in half of the *c*-stacked layers. The close-packed layers are parallel to (100) in the monoclinic structure and the periodicity of the stacking sequence is $a \sin\beta = 18.7$ Å. By analogy we considered that the HP phase had a four-layer stacking of close-packed layers, $(ch)_2$ with the stacking periodicity equal to $c = 8.614$ Å. This gives a separation between close-packed layers of $c/4 = 2.15$ Å which compares closely with the close-packed layer repeat of 2.16 Å in corundum (11). On the basis of a close-packed anion model for the HP phase the *a* parameter of 7.223 Å can then be assigned as $\sqrt{7} \times$ O–O, corresponding to an anion–anion separation of 2.73 Å in the close-packed layers. This compares closely with an anion–anion separation of 2.75 Å in corundum (11).

A close-packed structure with a $\sqrt{7} \times$ O–O basal plane parameter comprises 7 anions per layer, giving 28 anions per unit cell, of which one is replaced by Ca by analogy with the Ba–Ti ferrite. Assuming the Al and Si atoms occur in integral proportions in the unit cell, then charge balance requirements give a number of possible unit cell compositions, of which only one is close to the approximate composition determined by microprobe analysis. It is $CaAl_{12}Si_4O_{27}$.

The space group for four-layer (*chch*) anion close-packing is $P6_3/mmc$. Subgroups of this space group which have a 1-fold site to accomodate the Ca are *P*-6 and *P*-3. The space group *P*-6 would require the Ca to occupy an *h*-stacked anion layer whereas the space group *P*-3 allows the Ca to be in the *c*-stacked layer. The latter was chosen by analogy with the situation in $BaFe_{11}Ti_3O_{23}$. The location of the Ca in one of the *c*-stacked anion layers restricted the possible interstitial sites that could be occupied by Al and Si. It was a straightforward matter then to establish a distribution of the 12 Al and 4 Si atoms in three octahedral sites and one tetrahedral site that gave a good qualitative match to the PXRD pattern and provided a starting model for the Rietveld refinement.

Structure Refinement

Once the correct composition was established, further HP syntheses were undertaken using the appropriate molar ratios of starting materials to obtain a pure phase for structure refinement. This proved to be difficult. The product purity was sensitive to the preparation conditions, particularly the homogeneity of the starting glass, and minor amounts of other phases were always present. These included $CaAl_4Si_2O_{11}$, kyanite, grossular garnet, and corundum. The cleanest preparation was from a reaction of a 1:6:4 molar ratio at 1550°C and 14 GPa for 2 h. The PXRD pattern showed corundum as the most significant impurity phase together with a trace of garnet. This product was used for the Rietveld refine-

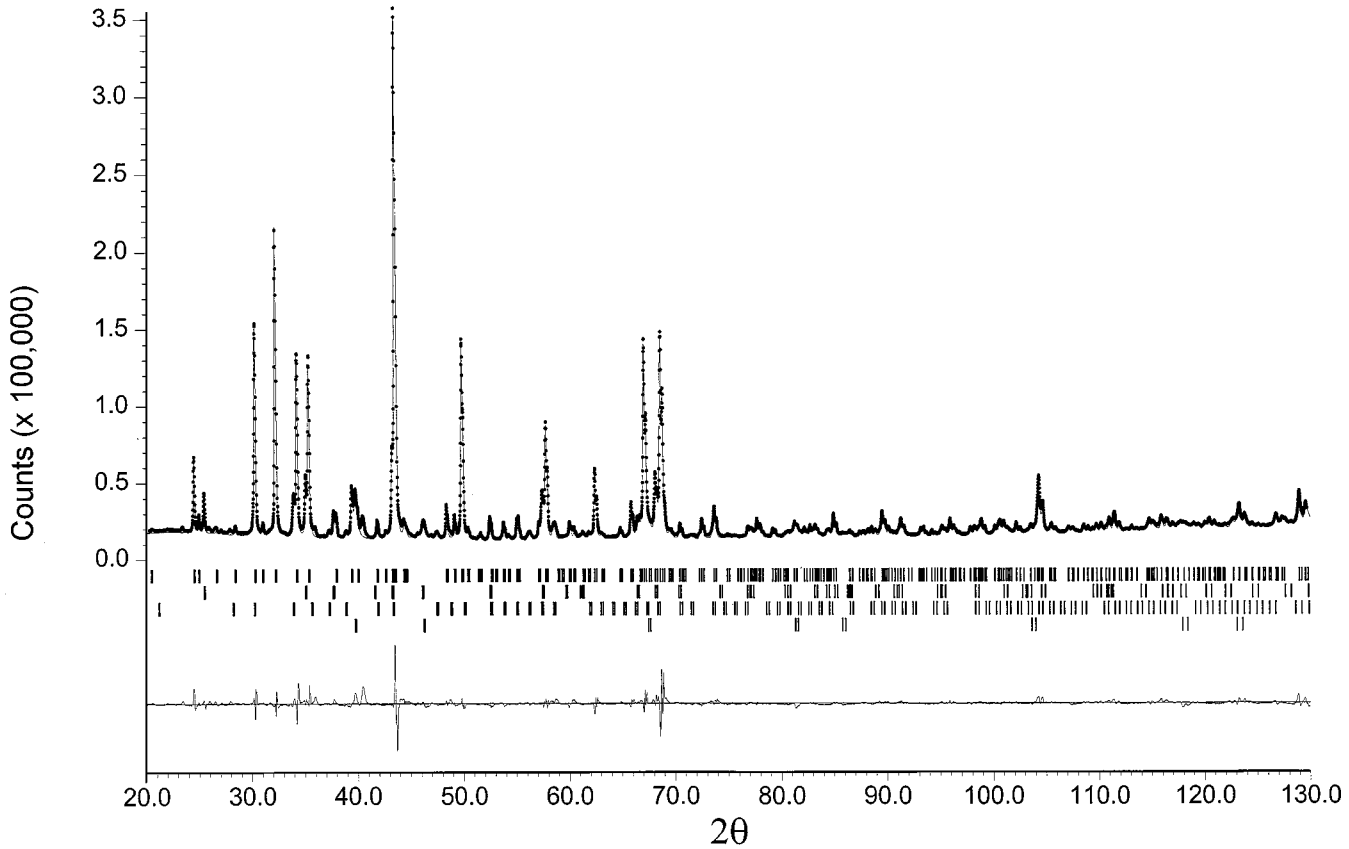

FIG. 1. Observed (dots), calculated (line), and difference plots from Rietveld refinement for $CaAl_{12}Si_4O_{27}$. The rows of tic marks show the positions of the allowed Bragg reflections for, from top to bottom, $CaAl_{12}Si_4O_{27}$, corundum, grossular, and platinum.

ment and the impurity phases were included in the refinement.

Initially the Si and Al atoms were distributed randomly over two 6-fold and two 2-fold cation sites in space group *P*-3. After convergence of the refinement, the isotropic thermal parameters showed large positive and negative values that suggested ordering of the Si in the 2-fold sites and Al in the 6-fold sites. The ordering was confirmed by bond valence calculations (12). The refinement was continued using the ordered model. The final refinement involved 23 profile parameters, 27 coordinates and isotropic *B* values for $CaAl_{12}Si_4O_{27}$, and 483 unique Bragg reflections. Convergence was achieved at $R_{wp} = 6.1\%$ and $R_B = 2.7\%$. The refined amounts of corundum and grossular were 10.3 wt% and 2.8 wt%, respectively. On the basis that the dominant phase, $CaAl_{12}Si_4O_{27}$, has the same composition as the bulk sample, the quantitative phase analysis indicates that some SiO_2 or a silica-rich phase should also be present. Silica polymorphs including the HP form, stishovite, could not be identified in the PXRD pattern, and so the silica-rich phase, if present, is either amorphous or below the limit of detection.

The refined coordinates and isotropic *B* values for $CaAl_{12}Si_4O_{27}$ are reported in Table 1, together with calculated valence sums at the different metal atom and oxygen sites. Important interatomic distances are given in Table 2. Observed and calculated PXRD patterns are shown in Fig. 1.

RESULTS AND DISCUSSION

Description of Structure

The structure of $CaAl_{12}Si_4O_{27}$ is composed of two compositionally similar but structurally distinct layer motifs. These are illustrated in a projection along [001] in Fig. 2 One layer, Fig. 2a, is composed of triangular clusters of edge-shared $Al(1)O_6$ octahedra that are connected via edge-sharing with $Si(1)O_6$ octahedra to form nine-member rings. Pairs of such layers are interconnected across a *c*-stacked CaO_6 anion layer by edge-sharing. The Ca atoms sit at the centers of the nine-member rings. These double layers can be alternatively described as being composed of $[SiAl_3O_{16}]^{19-}$ tetrahedral clusters of octahedra that are interconnected by edge-sharing. Each nine-member ring is formed from six such clusters, three with the Si apex pointing along [001] alternating with three having the apex pointing in the opposite direction. The double layer is shown in Fig. 3a.

TABLE 1
Rietveld Refinement Results and Valence Sums for $CaAl_{12}Si_4O_{27}$

Atom	Site and symmetry	x	y	z	B (Å^2)	Calculated valence[a] (Ref. 12)
Ca	1(*a*) (− 3)	0	0	0	1.3(1)	1.52
Al(1)	6(*g*) (1)	0.0852(5)	0.4508(5)	0.1343(4)	0.61(8)	3.20
Al(2)	6(*g*) (1)	0.2581(5)	0.2064(4)	0.3518(5)	0.60(7)	2.88
Si(1)	2(*d*) (3)	1/3	2/3	0.8636(9)	0.3(1)	4.05
Si(2)	2(*d*) (3)	1/3	2/3	0.4467(7)	0.3(1)	4.08
O(1)	6(*g*) (1)	0.4572(8)	0.1515(9)	0.0012(9)	0.80(5)	2.04 (2.33)
O(2)	6(*g*) (1)	0.045(2)	0.231(1)	0.2452(6)	0.80(5)	2.06 (1.67)
O(3)	2(*d*) (3)	1/3	2/3	0.247(1)	0.80(5)	2.12 (2.5)
O(4)	6(*g*) (1)	0.494(1)	0.386(1)	0.2375(6)	0.80(5)	1.96 (1.67)
O(5)	1(*b*) (− 3)	0	0	1/2	0.80(5)	1.63 (3.0)
O(6)	6(*g*) (1)	0.4252(8)	0.170(1)	0.5092(8)	0.80(5)	1.98 (2.0)

Note: Refinement in *P*-3, $a = 7.223(1)$ and $c = 8.614(3)$ Å, $R_{wp} = 6.1\%$, $R_B = 2.7\%$. Impurity phases: Al_2O_3 (corundum), 10.3 wt%; $Ca_3Al_2Si_3O_{12}$ (grossular), 2.8 wt%.

[a] Values in parentheses are Pauling valences = $\sum$ (metal valence)/coordination.

The second type of layer, shown in Fig. 2b, is also composed of triangular clusters of edge-shared Al-centered octahedra (containing Al(2)), but in this case the groups are interconnected within the layer by corner-sharing to $Si(2)O_4$ tetrahedra. Pairs of such layers are interconnected across a *c*-stacked oxygen layer by edge-sharing of the octahedra, giving octahedral clusters of octahedra, $[Al_6O_{19}]^{20-}$, as illustrated in Fig. 3b. The two different types of layer motifs are interconnected across *h*-stacked oxygen layers by corner-sharing of the polyhedra as illustrated in Fig. 4. A side-on view of the layer stacking is shown in Fig. 5.

The structure contains both four-coordinated and six-coordinated silicon. The four-coordinated Si(2) is unusual in having one very long bond, Si(2)–O(3) = 1.718 Å. O(3) is coordinated also to three Al(1) atoms and so is oversaturated with a formal valence of 2.5. All four M–O(3) distances are elongated to reduce the calculated valence sum at O(3) to 2.12, see Tables 1 and 2. The other three Si(2)–O distances, to O(6), are shorter than normal and the resulting valence sum calculated at Si(2) is close to that expected for silicon at 4.08. The valence sum at the octahedrally coordinated Si(1) is also close to that expected at 4.05.

TABLE 2
Selected Interatomic Distances (Å) in $CaAl_{12}Si_4O_{27}$

Al(1)–O(1)		1.883(7)	Al(2)–O(2)		1.862(10)
–O(1)		1.956(8)	–O(2)		1.876(14)
–O(1)		1.960(8)	–O(4)		1.829(6)
–O(2)		1.748(9)	–O(5)		2.133(3)
–O(3)		1.947(5)	–O(6)		1.919(8)
–O(4)		1.858(8)	–O(6)		1.991(7)
Si(1)–O(1)	(×3)	1.839(8)	Si(2)–O(3)		1.720(10)
–O(4)	(×3)	1.712(9)	–O(6)	(×3)	1.588(5)
Ca–O(1)	(×6)	2.914(6)			
–O(2)	(×6)	2.609(7)			
Al(1)–Al(1)	(×2) edge	2.923(4)	Al(2)–Al(2)	(×2) edge	2.959(4)
–Al(1)	edge	2.872(8)	–Al(2)	(×2) edge	3.072(7)
–Si(1)	edge	2.701(4)	–Si(2)	corner	3.139(5)
–Si(1)	edge	2.878(7)	–Si(2)	corner	3.195(4)
–Al(2)	corner	3.191(5)			
–Si(2)	corner	3.176(5)			

The Al-centered octahedra are relatively distorted as shown by the bond length ranges for Al(1)–O and Al(2)–O in Table 2. However the distances are within the ranges reported for close-packed aluminate structures (13, 14), and the variations are consistent with the variations in formal valences at the different anion sites, with short distances to undersaturated O(2) and O(4) and long distances to oversaturated O(1) and O(5), see Tables 1 and 2. The Al(2)–O(5) distance is particularly long. This oxygen is coordinated to six metal atoms as in the rocksalt structure and its formal valence sum is 3. The displacements of the Al(2) atoms to give Al(2)–O(5) = 2.133 Å overcompensate for this oversaturation, giving a calculated valence sum at O(5) of only 1.63. Clearly factors other than bonding to O(5) are controlling the displacements of the Al(2) atoms, in particular their mutual repulsion across the shared edges in the Al_6O_{19} clusters.

The coordination of Ca is strongly deformed from cuboctahedral, with the distances to the apical oxygens O(2) at close to the optimum Ca–O distance for 12-coordination of 2.63 Å but with distances to the axial oxygens O(1) almost 0.3 Å longer. The long Ca–O(1) distances result from the constraint imposed on the location of O(1) due to repusion of Al(1), Si(1) atoms across shared O(1)–O(1) edges. This

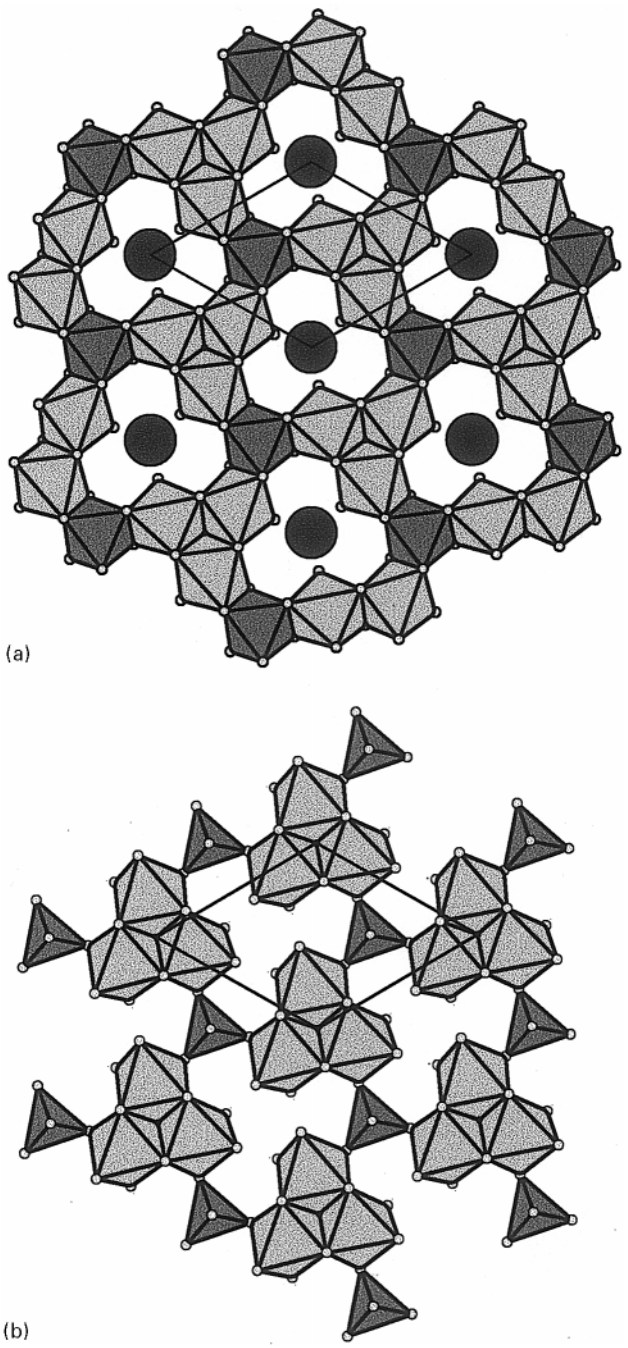

FIG. 2. Polyhedral representation of (001) layers containing (a) $Al(1)O_6$ and $Si(1)O_6$ octahedra and (b) $Al(2)O_6$ octahedra and $Si(2)O_4$ tetrahedra, viewed along [001]. Large circles are Ca atoms. The unit cell outline is shown.

results in marked O(1)–O(1) edge-shortening to 2.47 Å in the basal plane containing O(1) and Ca, with a corresponding displacement of O(1) away from the Ca site. The calculated valence sum at the Ca site is only 1.52. This is typical of valence sums for Ca substituted at an anion site in close-packed oxide structures, for example 1.35 in $Ca_2Zn_4Ti_{16}O_{38}$ (15) and 1.50 in hibonite, $CaAl_{12}O_{19}$ (13), which is due to the Ca^{2+} ion being too small for this type of site. The "rattling" of Ca in the anion site is also reflected in its high B value of 1.3 $Å^2$. A better size match for Ca is obtained in the close-packed HP phase $CaAl_4Si_2O_{11}$, for

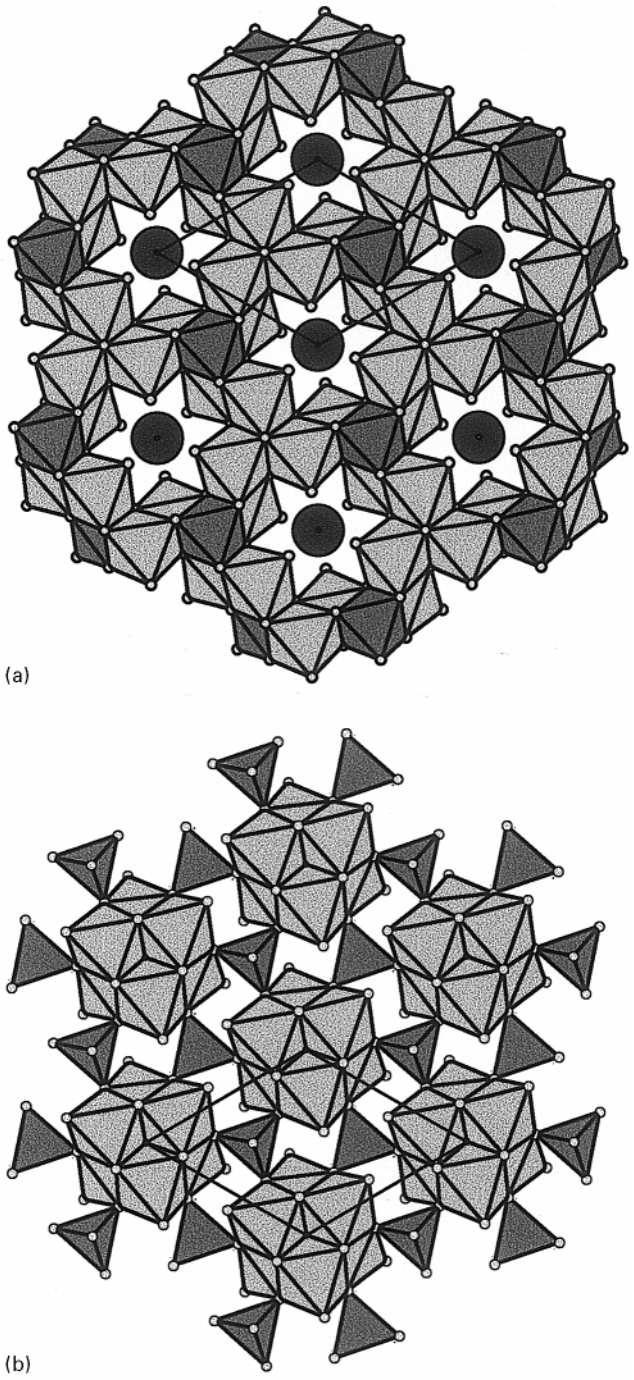

FIG. 3. Polyhedral representation of adjacent pairs of (001) layers across (a) the cubic-stacked CaO_6 layer at $z = 0$ and (b) the cubic-stacked O_7 layer at $z = 0.5$. Large circles are Ca atoms.

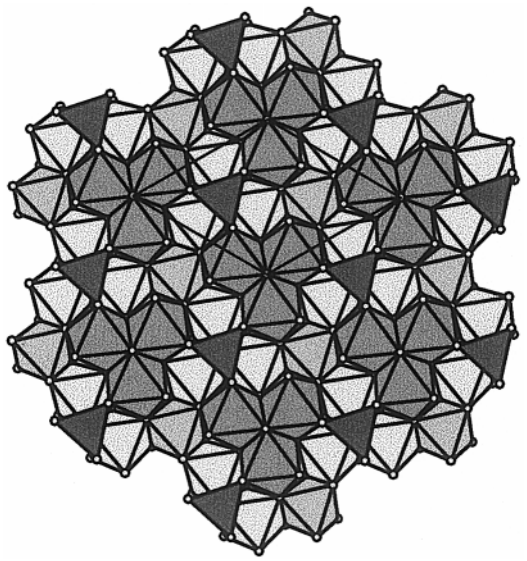

FIG. 4. Polyhedral linkages across the hexagonal-stacked anion layers, viewed along [001].

which the valence sum is 1.78 (1). This is due to a denser packing for the more Si-rich compound. The calculated density for $CaAl_4Si_2O_{11}$ is 3.91 g/cm^2, compared to a density of 3.87 g/cm^3 for $CaAl_{12}Si_4O_{27}$. Both compounds have considerably higher densities than that for grossular garnet, 3.60 g/cm^2, which was often found as a coexisting phase in the quenching experiments (1).

Comparison with Other Structures

The observed similarity between the PXRD patterns for $CaAl_{12}Si_4O_{27}$ and $BaFe_{11}Ti_3O_{23}$ assisted in the structure determination of the HP phase, and in fact the two structures have many features in common. These include the same *ch* stacking sequence of close-packed anion layers with the large cation occupying half of the *c*-stacked layers, the occupation of tetrahedral sites with their bases in the other half of the *c*-stacked layers, and the grouping of octahedra into triangular edge-shared clusters. The main structural differences derive from the packing density of the large cation in the *c*-stacked anion layers and its relative location in successive layers. The layer composition is CaO_6 for the HP phase and BaO_5 for the ferrite. This engenders a different distribution of cations in the octahedral sites. In both structures triangular groupings are the basic units in individual layers, but in the HP phase these groupings of octahedra are either isolated or link via other octahedra into nine-member rings whereas in the ferrite they join by edge-sharing to form zig–zag columns.

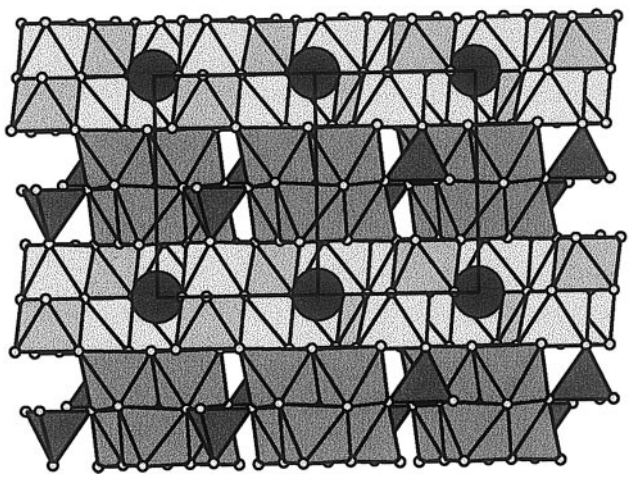

FIG. 5. A view along [100] of the stacking of polyhedra in $CaAl_{12}Si_4O_{27}$. Large circles are Ca atoms. The unit cell outline is shown, with [001] vertical.

A most distinctive feature of the structure of $CaAl_{12}Si_4O_{27}$ is the presence of Al_6O_{19} octahedral clusters of edge-sharing octahedra, effectively an element of the rocksalt structure. This type of cluster is well known in niobates. For example, the presence of Nb_6O_{19} clusters has been reported in $Na_7(H_3O)Nb_6O_{19}.14H_2O$ (16). In this compound the Nb is pentavalent and the formal valence sum at the oxygen site at the center of the cluster is 5. Large displacements of the Nb atoms away from the cluster center (Nb–O = 2.38 Å) occur to give a better local charge balance. More commonly in niobates however, the niobium is in a reduced valence state and is involved in metal–metal bonding which draws the Nb atoms closer together. In these cases the central oxygen is missing, giving a Nb_6O_{18} cluster (17).

The nine-member rings of edge-shared octahedra found in $CaAl_{12}Si_4O_{27}$ occur also in the aluminum tantalate mineral simpsonite, $Al_4Ta_3O_{13}(OH)$ (18). In fact simpsonite has the same basal plane dimensions $= \sqrt{7} \times$ O–O, with seven anions per layer, as for $CaAl_{12}Si_4O_{27}$. The anion layers in simpsonite have hexagonal stacking, giving a two-layer repeat. Isolated triangular clusters of octahedra in one layer link by corner-sharing to the octahedra forming the nine-member rings in adjacent layers. This is identical to the arrangement across the *h*-stacked layers in $CaAl_{12}Si_4O_{27}$ as shown in Fig. 4. However the HP phase also has tetrahedra forming in-plane corner connectivity between the triangular clusters.

The characterization of the new HP phase, with a structure related to that of $BaFe_{11}Ti_3O_{23}$, extends the analogy between the system BaO–Fe_2O_3–TiO_2 under ambient conditions and the system CaO–Al_2O_3–SiO_2 at high pressure where SiO_2 has the rutile-type structure. We have previously reported on the isostructural relation between $CaAl_4Si_2O_{11}$ and $BaFe_4Ti_2O_{11}$ (1). Structural analogies are also known for the magnetoplumbite-type $AM_{12}O_{19}$ (13) and hollandite-type AM_8O_{16} (19) structures in both systems. In view of the great diversity of structure types found

recently in the $BaO–Fe_2O_3–TiO_2$ system (19), the likelihood of finding further new phases at high pressure in the $CaO–Al_2O_3–SiO_2$ system is high, and lends impetus to further studies on this geologically important system.

REFERENCES

1. I. E. Grey, I. C. Madsen, H. St. C. O'Neill, S. E. Kesson, and W. O. Hibberson, *N. Jb. Miner Mh.* **1999,** 104 (1999).
2. L. Gautron, J. D. Fitzgerald, S. E. Kesson, R. A. Eggleton, and T. Irifune, *Phys. Earth Planet. Int.* **102,** 223 (1997).
3. X. Obradors, A. Collomb, J. Pannetier, A. Isalgue, J. Tejada, and J. C. Joubert, *Mater. Res. Bull.* **18,** 1543 (1983).
4. T. A. Vanderah, W. Wong-Ng, B. H. Toby, V. M. Browning, R. D. Shull, R. G. Geyer, and R. S. Roth, *J. Solid State Chem.* **143,** 182 (1999).
5. E. Ohtani, T. Irifune, W. O. Hibberson, and A. E. Ringwood, *High Temp. High Press.* **19,** 523 (1987).
6. R. J. Hill and C. J. Howard, *J. Appl. Crystallogr.* **18,** 173 (1985).
7. D. B. Wiles and R. A. Young, *J. Appl. Crystallogr.* **14,** 149 (1981).
8. G. Caglioti, A. Paoletti, and F. P. Ricci, *Nucl. Instrum.* **3,** 223 (1958).
9. "International Tables for X-Ray Crystallography," Vol. IV. Kynoch Press, Birmingham, 1974.
10. J. W. Visser, *J. Appl. Crystallogr.* **2,** 89 (1969).
11. A. S. Brown, M. A. Spackman, and R. J. Hill, *Acta Crystallogr. Sect. A* **49,** 513 (1993).
12. N. E. Brese and M. O'Keeffe, *Acta Crystallogr. Sect. B* **47,** 192 (1991).
13. K. Kato and H. Saalfeld, *Naturwissenschaften* **1967,** 536 (1968).
14. W. A. England, A. J. Jacobson, and B. C. Tofield, *Solid State Ionics* **6,** 21 (1982).
15. B. M. Gatehouse and I. E. Grey, *J. Solid State Chem.* **46,** 151 (1983).
16. A. Goiffon, E. Philippot, and M. Mourin, *Rev. Chim. Miner.* **17,** 466 (1980).
17. K. B. Kersting and W. Jeitschko, *J. Solid State Chem.* **93,** 350 (1991).
18. T. S. Ercit, P. Cerny, and F. C. Hawthorne, *Can. Mineral.* **30,** 663 (1992).
19. T. A. Vanderah, J. M. Loezos, and R. S. Roth, *J. Solid State Chem.* **121,** 38 (1996).